

MINISTRY OF INDUSTRY
AND TRADE

MINISTRY OF EDUCATION
AND TRAINING

NARIME

NGUYEN THAI SON

**RESEARCH ON THE EFFECTS OF SELECTED PROCESS
PARAMETERS ON THE QUALITY OF 3D PRINTED – SLM
PARTS FROM Ti6Al4V MATERIAL**

SUMMARY OF DOCTORAL THESIS

Industry: Mechanical Engineering

Item No.: 9520103

Hanoi – 2026

The project was completed at:
**National Research Institute Of Mechanical Engineering – Ministry
of Industry and Trade**

Scientific Instructor:

- 1. Assoc. Prof. Dr. Tran Ngoc Hien**
- 2. Assoc. Prof. Dr. Nguyen Chi Sang**

Critic 1: Prof. Dr. Nguyen Duc Toan

Critic 1: Assoc. Prof. Dr. Hoang Tien Dung

Critic 1: Assoc. Prof. Dr. Hoang Van Got

**The thesis is defended before the Institute-level doctoral thesis evaluation
council**

Meeting at: National Research Institute Of Mechanical Engineering - Ministry
of Industry and Trade

Head Office Building: No. 4 Pham Van Dong Street, Cau Giay District, Hanoi
City

At 8h30 (hours), on 3 (month) 14 (day), 2026 (year)

The thesis can be found at:

- 1. National Library of Vietnam**
- 2. Library of the National Research Institute Of Mechanical Engineering**

INTRODUCTION

1. Rationale for selecting the dissertation topic

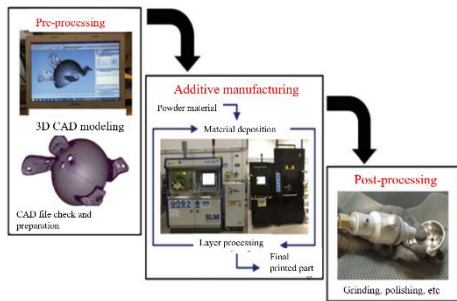
Together with the development of intelligent manufacturing systems aimed at improving productivity and quality of traditional subtractive machining processes, the additive manufacturing systems are also being widely and increasingly applied. While subtractive machining removes material from a workpiece to form a part, additive manufacturing builds the part by adding material layer by layer. Figure 0.1 illustrates the additive manufacturing process, includes steps from processing the part's CAD model on a computer, to 3D printing the part on a 3D printer, then finally post-processing to achieve the required product quality.

Additive manufacturing technology enables the fabrication of products with complex geometries and a wide variety of product types; therefore, it has been continuously studied and improved to expand its range of applications. However, product quality remains one of the major barriers to the widespread adoption of additive

manufacturing technology. One of the solutions that is being investigated to ensure printing quality is the identification of appropriate printing process parameters in order to satisfy the output criteria such as surface quality, dimensional accuracy, and mechanical properties of the products.

Nevertheless, currently there are many different printing methods for different materials, and the output criteria also depend on specific applications, leading to different requirements. Therefore, research on product quality during the printing process is essential for practical applications.

Selective Laser Melting (SLM) is an additive manufacturing method for metal powder materials. Nowadays, the SLM is widely used due to its many advantages. Numerous studies have been conducted on various application-oriented problems using Ti-6Al-4V powder material fabricated by the SLM process, focusing on ensuring the quality of printed products in relation to printing process parameters. However, most studies concentrated on the effects of laser power and scanning speed while keeping the fixed layer thickness, even though variations in layer thickness also influence the quality of the printed products. Moreover, the combined effects of process parameters on geometric deviation, surface roughness, and porosity-free printed area have not yet been evaluated simultaneously. This constitutes a research gap that requires to be addressed in order to determine the optimal process parameters and ensure the quality of printed products in practical applications.



From the above analyses, the topic “**Investigation of the effects of selected process parameters on the quality of 3D-printed SLM parts made from Ti-6Al-4V material**” can be considered novel and necessary. This research not only contributes to enriching the theoretical foundation of SLM printing for difficult-to-machine materials, but also opens up prospects for practical applications in additive manufacturing to manufacture complex-shaped components in the industrial and medical fields.

2. Research objectives of the dissertation

- To develop mathematical models describing the relationships between printing process parameters and the quality indicators of printed products.
- To determine the optimal set of printing process parameters that satisfies the required output criteria.

3. Research object and scope

- **Research object:** Investigation of the effects of three input parameters, including laser power, scanning speed, and layer thickness, on geometric accuracy, surface roughness, and porosity in metal 3D printing.
- **Research scope:** Metal 3D printing technology applied to the fabrication of components from Ti-6Al-4V titanium alloy powder with an average particle size of 43 μm using the Selective Laser Melting (SLM) process.

4. Research methodology

Based on the above objectives, research object and scope, the research procedures are illustrated in Figure 0.2, combining theoretical analysis, numerical simulation, and experimental methods.

5. Scientific and practical significance of the topic

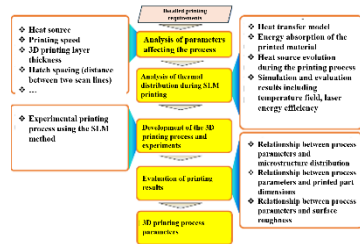
* Scientific significance:

- Clarifying the main process parameters that influence the Selective Laser Melting (SLM) process for Ti-6Al-4V titanium alloy powder.
- Establishing heat source models and heat transfer models, and analyzing temperature distribution during printing as a basis for determining appropriate printing process parameters.

- Developing mathematical models that describe the relationships between output quality indicators and printing process parameters, providing a scientific basis for selecting suitable process parameters for specific output requirements in practical applications.

* **Practical significance:**

- The research results on the relationships between the printed product quality indicators and the printing process parameters enable the determination of appropriate process parameters set to achieve the desired output quality in practical applications.



- The research results can serve as teaching and research materials, as well as a reference for enterprises applying additive manufacturing technology to improve product quality.

6. Novel contributions of the dissertation

1. Further development and refinement of the theoretical framework for metal 3D printing processes applied to Ti-6Al-4V titanium alloy powder.

2. Simulation-based analysis of the thermal process during printing, from which the temperature distribution state can be predicted to ensure appropriate material melting conditions corresponding to specific sets of printing process parameters.

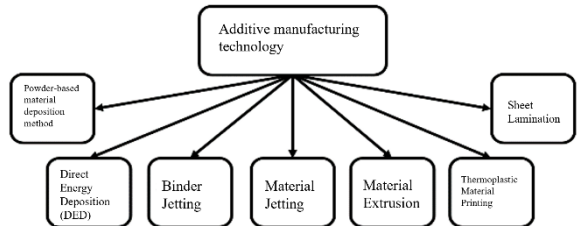
3. Development of predictive models for printed product quality, including geometric deviation, surface quality, and porosity, in relation to printing process parameters via experimental studies using the SLM process. Based on these models, optimal process parameter sets were determined to ensure product quality under single-objective or multi-objective optimization criteria (minimum surface roughness, minimum geometric deviation, and maximum porosity-free printed area).

CHAPTER 1. OVERVIEW OF ADDITIVE MANUFACTURING AND THE SLM PROCESS FOR Ti-6Al-4V MATERIAL

1.1. Overview of additive manufacturing

According to the definition of the American Society for Testing and Materials (ASTM), “Additive manufacturing is a process of joining materials to make three-dimensional objects, usually by building them layer upon layer, as opposed to subtractive manufacturing methodologies traditionally used” [1]. Additive manufacturing (AM), also referred to as layer-by-layer manufacturing or 3D printing, has been effectively applied in numerous fields. AM has been continuously studied and improved and has become one of the core technologies of the Fourth and Fifth Industrial Revolutions [2–4].

In current manufacturing systems, a 3D model is designed using CAD software and then transferred to CAM software to establish toolpaths and processing parameters, from which G-code is generated for execution on CNC machines. Additive manufacturing can be classified based on the method of part formation; the type of printing material such as solid, powder, or liquid; and the thermal energy source used for processing. According to these criteria, AM technologies are categorized into seven groups.



The powder bed fusion (PBF) processes for metallic materials, as illustrated in Figure 1.7, include selective laser sintering (SLS), selective laser melting (SLM), and electron beam melting (EBM). Compared with SLS and EBM, the SLM process is more widely utilised in industrial applications.

With the advances in science and technology, additive manufacturing enables rapid fabrication of prototypes and customized components. Currently, a wide range of 3D printers employing different materials and processes are available; therefore, the selection of a printing technology depends on the intended application and the specific product requirements.

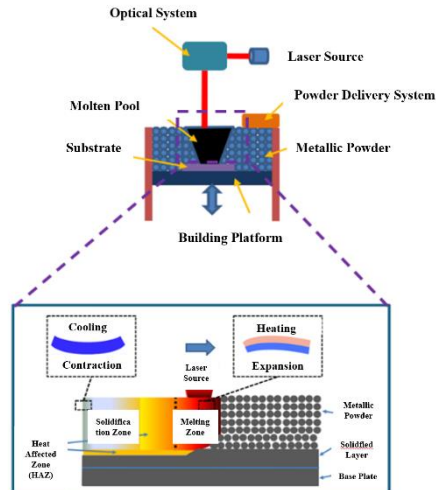
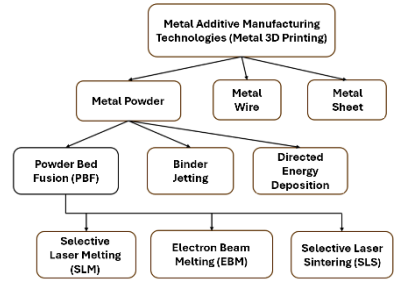
1.2. Product quality in additive manufacturing

The 3D printing process, particularly Selective Laser Melting (SLM), is influenced by numerous process parameters such as scanning speed, hatch pattern, and layer thickness. These factors directly affect printing quality, including surface roughness, geometric deviation, and mechanical properties. In this dissertation, simulation and experimental studies were conducted to evaluate the effects of parameters such as laser power, scanning speed, and layer thickness on dimensional accuracy, surface quality, and microstructure. Results have been obtained for both the Wire Arc Additive Manufacturing (WAAM) process and the SLM process.

1.3. Selective laser melting process

In additive manufacturing technology, Selective Laser Melting (SLM) is one of the processes used to fabricate products from metal powders [10].

Figure 1.9 illustrates the SLM printing mechanism. The printing process is carried out layer by layer: powder is deposited, melted by a laser beam, and then the build platform is lowered to repeat the procedure until the part is completed. Printed products shall meet requirements in terms of dimensional accuracy, geometric fidelity, surface quality, and mechanical properties. However, the rapid phase transitions from solid to liquid and back to solid during the SLM process significantly affect the product quality. Therefore,



optimization of the process to improve both quality and productivity remains a major research focus.

1.4. Overview of international research

1.4.1. Research Trends in Additive Manufacturing

Researches on additive manufacturing technologies have increased significantly in recent years. Among these, thermoplastic material printing, material extrusion, and direct energy deposition are the three processes with the largest number of protected patents. Most studies have focused on polymer materials.

Current research directions in metal 3D printing mainly include:

- Application-oriented research in specialized fields:

With ongoing studies aimed at improving printing quality and developing new materials, metal additive manufacturing—particularly using titanium alloys—has been increasingly applied in fields that require components with high technical performance.

- Application of artificial intelligence in additive manufacturing systems:

In current AM systems, product quality remains a critical issue. Recent studies indicate that integrating artificial intelligence into AM systems can improve product quality, reduce printing defects, and has been proposed for application in both the product design stage and the printing process.

- Development and updating of standards for additive manufacturing:

To implement AM systems in industrial applications, standardized frameworks are essential to establish common regulations. As of 2016, standards mainly focused on technical specifications for specific materials.

1.4.2. Research on Selective Laser Melting of Ti6Al4V Material

Ti6Al4V powder is widely used in the SLM process for manufacturing various products due to its high fatigue strength and excellent mechanical properties, which satisfy demanding service requirements.

Surface roughness and microstructural characteristics are critical quality indicators of printed components.

The quality of 3D-printed parts depends on four main groups of factors. In this study, via experimental investigations using SLM and Ti6Al4V material, the relationship between geometric accuracy and printing parameters was established. Based on regression models, optimal printing parameter sets were identified to minimize geometric deviation.

1.5. Overview of Domestic Research

1.5.1. State of the Art in Additive Manufacturing

According to statistical reports from the Information and Statistics Center for Science and Technology under the Ho Chi Minh City Department of Science and Technology on the status of research and application of 3D printing technology in Vietnam, current studies mainly focus on the following aspects [7]:

- Mastering the design and fabrication of 3D printers:

Most studies concentrate on the design and fabrication of 3D printers for polymer-based products.

Application-oriented research on 3D printing technology:

Research on effective applications of 3D printing technology in various fields is essential, especially for metal materials. A research group from the Military Technical Academy successfully carried out a Nafosted-funded research project. In the medical field, several major hospitals in Hanoi and Ho Chi Minh City have implemented 3D-printed products in surgical applications..

1.5.2. Research Status on Selective Laser Melting of Ti-6Al-4V Material

In order to improve the mechanical properties of SLM-printed Ti-6Al-4V components, a comprehensive review was conducted to evaluate the effects of heat treatment on mechanical properties and microstructure [41,42]. In addition, Nguyen Minh Thuyet et al. investigated the interaction between titanium substrates and Ti-6Al-4V powder, as well as experimentally studied the mechanical properties and microstructural characteristics of products fabricated using the SLS process [43,44].

Conclusion of Chapter 1

Based on the overview of additive manufacturing and the Selective Laser Melting (SLM) process using Ti-6Al-4V powder, the following conclusions can be drawn:

1-For additive manufacturing in general and the SLM process in particular, four main groups of factors influence the quality of printed products:;(1) Printing methods and printer accuracy;(2) Printing materials, including thermal properties and particle size distribution;(3) Printing parameters such as laser power, scanning speed, and layer thickness;(4) Printing conditions, including powder drying, protective atmosphere in the build chamber, and post-processing methods such as heat treatment, grinding, and polishing.

2- For the SLM process using Ti-6Al-4-V powder, studies on the effects of printing parameters on the product quality shall simultaneously consider key factors such as laser power, scanning speed, and layer thickness. Existing studies mainly focus on variations in laser power and scanning speed while keeping fixed layer thickness. Therefore, a research considering the simultaneous variation of these process parameters enables more a effective practical implementation by addressing both productivity requirements (larger layer thickness) and quality demands in order to determine the optimal process parameter sets.

3- Research on the SLM process for Ti-6Al-4-V powder shall focus on determining the combined effects of core process parameters (such as laser power, scanning speed, and layer thickness) on key output quality indicators, including geometric deviation (D), surface roughness (Ra), and microstructural characteristics, using dedicated experimental equipment.

CHAPTER 2. THEORETICAL BASIS OF METAL 3D PRINTING

2.1. Quality of Printed Products

The quality of printed products is evaluated based on geometric accuracy, surface quality, mechanical properties, aesthetic appearance, functional performance, compliance with standards, and safety requirements.

Printed product quality depends on many factors, among which the main influencing factors include the printing method, printing material, and printing process parameters. In this study, the focus is placed on geometric accuracy, surface quality, and mechanical properties.

2.1.1. Geometric Accuracy

One of the most important quality criteria for 3D-printed products is the dimensional and geometric accuracy, which refers to the degree of conformity between the physical dimensions and geometry of the printed product and the designed dimensions and geometry.

Geometric deviation of printed products is caused by the effects of thermal energy during the metal powder melting process and the rapid phase transitions from solid to liquid and back to solid. In addition, the geometric deviation is also influenced by factors such as printer settings, material properties, environment conditions, and post-processing techniques.

2.1.2. Surface Quality

Another important quality criterion for 3D-printed products is the surface quality, which refers to surface smoothness, roughness, or texture. Surface quality is affected by factors such as the printing method, layer height, nozzle size, scanning speed, and post-processing techniques.

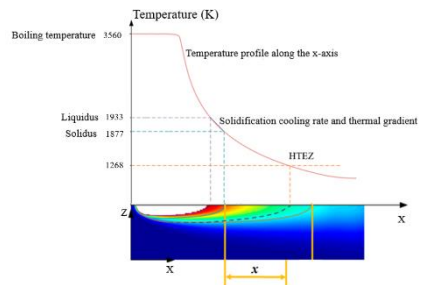
2.1.3. Mechanical Properties

The third important quality criterion for 3D-printed products is the mechanical properties, including strength, hardness, porosity, and fatigue strength. Mechanical properties are determined by factors such as material composition, printing method, build orientation, infill density, and post-processing techniques.

2.2. Phase Transformation Model of Metallic Materials during Printing

Figure 2.9 illustrates the phase transitions of Ti-6Al-4-V alloy as a function of temperature, from solid to liquid and vapor phases. From the phase transition diagram, it can be observed that the printing process parameters must generate temperatures higher than 1268 K to ensure proper layer formation.

After printing a layer, the material undergoes a phase transition from



solid to liquid and back to solid. During the rapid cooling stage (transition from liquid back to solid), the temperature range of Ti-6Al-4-V alloy from 1268 K to 1877 K constitutes the heat-affected thermal zone (HTEZ), where residual thermal stresses are present. The length of the heat-affected zone is determined as follows [54]:

$$x = 1.22\sqrt{\gamma \cdot t'} \quad (2.1)$$

where γ is the thermal diffusivity, and t' is the laser interaction time.

The relationship between thermal diffusivity and thermal conductivity is given as follows [54]:

$$\gamma = \lambda \cdot \rho \cdot C \quad (2.2)$$

where λ is the thermal conductivity (J/(m s K)), ρ is the material density (kg/m³), and C is the specific heat capacity (J/(kg K)).

The printing analysis model is divided into two regions, namely the first and second heat-affected thermal zones, depending on the degree of temperature variation. Subsequently, the temperature gradient (TG) is determined as the average temperature gradient of each zone.

The relationship between TG and material properties is expressed as follows [56]:

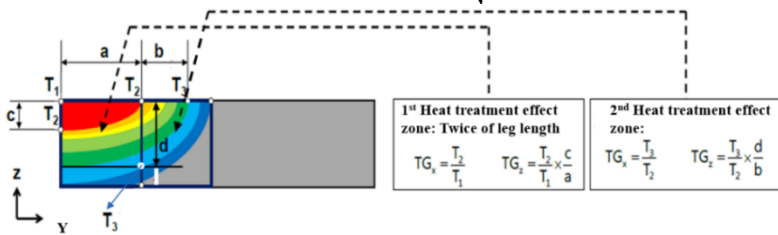
$$\Delta TG = |TG_{2nd\ HTEZ} - TG_{1st\ HTEZ}| = \frac{\rho \cdot m}{\alpha} \quad (2.3)$$

where ρ is the material density, m is the lattice parameter, and α is the coefficient of thermal expansion. At $T = 1173$ K, the value of m is $3.63 \cdot 10^{-7}$ (mm) [29]. The equation for calculating the material density based on the temperature gradient, lattice parameter, and thermal expansion coefficient is given by:

$$\rho = \frac{\Delta TG \cdot \alpha}{m} \quad (2.4)$$

Accordingly, the length of the heat-affected zone can be determined as:

$$x = 1.22\sqrt{\gamma \cdot t} = 1.22\sqrt{\lambda \cdot \rho \cdot C \cdot t} = 1.22\sqrt{\lambda \cdot \frac{\Delta TG \cdot \alpha}{m} \cdot C \cdot t} \quad (2.5)$$



To accurately determine the thermo-mechanical properties of printed parts, the phase transformations of the material during the SLM process, as well as the temperature-dependent material properties, must be considered. During heating, the phase transformation occurs from solid (metal powder) to liquid (molten powder), and from liquid to gas (vaporization) when the temperature exceeds the boiling point. During cooling, the phase transformation occurs from liquid to solid

to form the printed part. As phase transformations take place, the values of k (thermal conductivity), C (specific heat capacity), and ρ (density) also change and are calculated as follows [30]:

$$k = \theta k_{solid \rightarrow liquid} + (1 - \theta)k_{liquid \rightarrow gas} \quad (2.6)$$

$$C = \theta C_{rsolid \rightarrow liquid} + (1 - \theta)C_{liquid \rightarrow gas} \quad (2.7)$$

$$\rho = \frac{\theta \rho_{solid \rightarrow liquid} C_{solid \rightarrow liquid} + (1 - \theta) \rho_{liquid \rightarrow gas} C_{liquid \rightarrow gas}}{\theta C_{solid \rightarrow liquid} + (1 - \theta) C_{liquid \rightarrow gas}} \quad (2.8)$$

Where θ is the volume fraction ranging from 0 to 1 within the transition region. Assuming the temperature lies in the range from the sintering temperature (T_s) to the melting temperature (T_m), the values of k , C , and ρ are determined without considering the phase transition from liquid to gas.

$$k_{solid \rightarrow liquid} = \frac{k_{bulk} - k_{powder}}{T_m - T_s} (T - T_s) + k_{powder} \quad (2.9)$$

$$\rho_{solid \rightarrow liquid} = \frac{\rho_{bulk} - \rho_{powder}}{T_m - T_s} (T - T_s) + \rho_{powder} \quad (2.10)$$

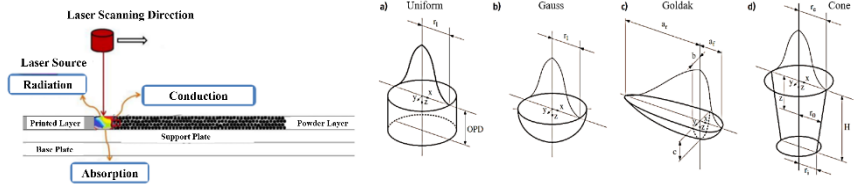
The density and thermal conductivity of the material in the powder state are calculated using the following equations. Where ρ_{bulk} and k_{bulk} are the density and thermal conductivity of the completely dense material (zero porosity):

$$\rho_{powder} = (1 - 0.43)\rho_{bulk} \quad (2.11)$$

$$k_{powder} = k_{bulk}(1 - 0.43)^4 \quad (2.12)$$

2.3. Heat transfer model in SLM process

When the laser source scans over the surface of the powder layer, energy is transferred from the top layer to the underlying layers through various physical phenomena, such as heat transfer, radiation, convection, thermal conduction, fluid flow in the melting pool, melting, evaporation, and chemical reactions [75].



The mathematical model describing the temperature distribution during the printing process, in relation to the thermal properties of the material and the processing parameters, is expressed as follows [33]:

$$\rho C \frac{\partial T}{\partial t} + \rho C V \nabla T = \nabla(k \nabla T) + Q_{\text{heat source}} \quad (2.13)$$

Where T is the temperature (K); ρ is the material density (kg/m³); C is the specific heat capacity J/(kg.K); k is the thermal conductivity (W/(m.K)); V is the scanning velocity (m/s); $Q_{\text{heat source}}$ is the laser energy distributed within the printed region of the layer (W/m³).

The laser energy distributed to the printed region is given by:

$$Q_{\text{heat source}} = Q_{\text{required power}} + Q_{\text{conduction}} \quad (2.14)$$

$$Q_{\text{required}} = Q_{\text{laser source}} - Q_{\text{convection}} - Q_{\text{radiation}} - Q_{\text{heat conduction}} \quad (2.15)$$

The required laser power is given by:

$$Q_{\text{required}} = Q \frac{6\sqrt{3}}{ab\pi\sqrt{\pi}} e^{\left[\frac{-3z^2}{b^2} + \frac{-3y^2}{a^2}\right]} \left[\frac{f_f}{c_f} e^{\frac{-3x^2}{c_f^2}} + \frac{f_r}{c_r} e^{\frac{-3x^2}{c_r^2}} \right] \quad (2.16)$$

The required laser power according to the Gaussian model is determined as follows:

$$Q_{\text{required}} = 2Q \frac{6\sqrt{3}}{a^2 b \pi \sqrt{\pi}} e^{\left[\frac{-3z^2}{b^2} + \frac{-3y^2}{a^2} + \frac{-3x^2}{a^2}\right]} \quad (2.17)$$

Determination of Laser Energy

In the SLM process, the thermal expansion occurring within the printed part layers may lead to deformation. The printing process quality is ensured depending on the excessive laser energy. Considering process parameters, the energy density E_v (J/mm^3) is calculated as follows [60]

$$E_v = \frac{Q_{\text{melting energy}}}{V \cdot t \cdot h_a} \quad (2.18)$$

where V is the scan speed (mm/s), h_a is the hatch spacing (mm), and t is the layer thickness (mm).

From the melting energy density, the required laser source energy is calculated as:

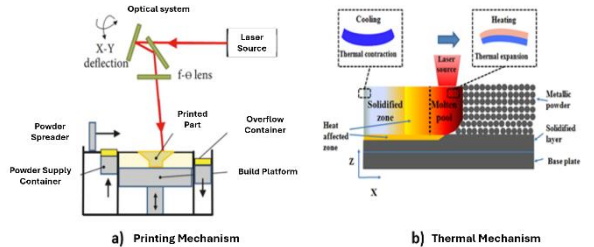
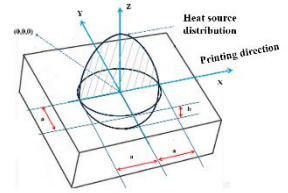
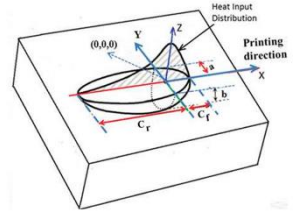
$$Q_{\text{laser source}} = Q_{\text{melting energy}} + \Delta Q \quad (2.19)$$

ΔQ represents the laser energy losses, including losses due to heat conduction, convection, radiation, and reflection at the material surface. To determine the laser energy required for melting the powder, the laser energy

efficiency (η) is defined as $\eta = \frac{Q_{\text{melting energy}}}{Q_{\text{laser source}}}$ (2.20)

2.4. SLM Mechanism

The SLM process utilizes a fine powder system to distribute a layer of 20-100 μm powder onto a substrate plate within a chamber filled with inert gas. Subsequently, this layer is fused by scanning a laser beam across the powder surface. High-intensity laser energy completely melts the metal powder to create solid metal. This process is repeated layer-by-layer until the component is completed.



The nature of the laser heating process for a powder layer differs significantly from that of a solid bulk for two reasons. First, the laser absorption of powder layers is considerably higher than that of bulk materials due to their different density and morphology [61], [62]. Second, the thermal conductivity of the powder layer is much lower than that of the bulk material because the contact area between powder particles is limited; therefore, heat transfer is dominated by the low thermal conductivity of the gas [63]. Due to these differences, it can be inferred that changing the diameter and packing density of the powder can significantly affect the thermal conductivity characteristics in SLM.

Due to the cyclic heating and cooling process in SLM, the total strain is calculated as the sum of its components: elastic strain and thermal residual strain (inelastic strain), represented by the formula:

$$\varepsilon_{total} = \varepsilon_{elastic} + \varepsilon^* \quad (2.21)$$

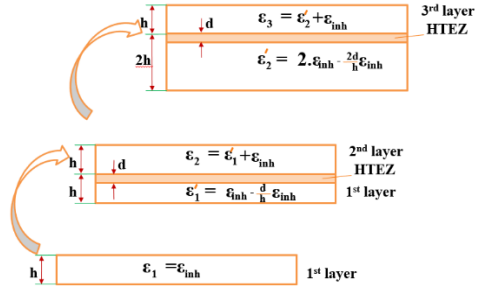
In which: $\varepsilon_{elastic}$: is Elastic strain; ε^* : is Thermal residual strain.

The value of thermal residual strain is determined by the following formula:

$$\varepsilon^* = \varepsilon_{thermal} + \varepsilon_{plastic} + \varepsilon_{phase\ transformation} + \varepsilon_{creep} \quad (2.22)$$

2.4.1. Multi-layer Printing Process

After completing the first printed layer, the inherent strain value at the Inherent Strain IS zone is ε_{inh} . The printer will continue to deploy the printing of layers 2, 3, up to layer n. The method for calculating inherent strain for n layers is illustrated in the following figure:



When printing the second layer, the first layer is re-melted with a new Heat Affected Zone, therefore, the remaining IS value for the first layer is:

$$\varepsilon'_1 = \varepsilon_{inh} - \frac{d}{h} \varepsilon_{inh} \quad (2.27)$$

Then, when the second layer is added, the IS value of this layer is:

$$\varepsilon_2 = \varepsilon'_1 + \varepsilon_{inh} = 2\varepsilon_{inh} - \frac{d}{h} \varepsilon_{inh} \quad (2.28)$$

When the third layer is added, the new IS value of the second layer becomes:

$$\varepsilon'_2 = \varepsilon_2 - \frac{d}{h} \varepsilon_{inh} = 2\varepsilon_{inh} - \frac{2d}{h} \varepsilon_{inh} \quad (2.29)$$

And the IS value in the third layer is calculated as follows:

$$\varepsilon_3 = \varepsilon'_2 + \varepsilon_{inh} = 3\varepsilon_{inh} - \frac{2d}{h} \varepsilon_{inh} \quad (2.30)$$

By repeating this SLM process for n layers, we can calculate the IS value for n layers as follows:

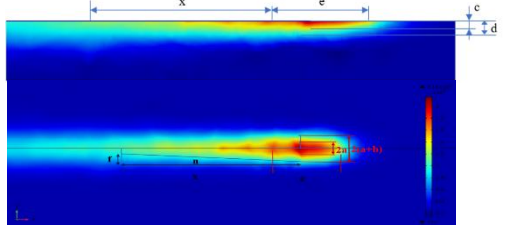
$$\varepsilon_n = \varepsilon'_{n-1} + \varepsilon_{inh} = n\varepsilon_{inh} - \frac{(n-1)d}{h} \varepsilon_{inh} \quad (2.31)$$

Regarding the total values along the x, y, and z axes, we obtain the following IS values:

$$\begin{cases} \varepsilon_x (n \text{ l\acute{o}p in}) = n\varepsilon_{inh-x} - \frac{(n-1)d}{h} \varepsilon_{inh-x} \\ \varepsilon_y (n \text{ l\acute{o}p in}) = n\varepsilon_{inh-y} - \frac{(n-1)d}{h} \varepsilon_{inh-y} \\ \varepsilon_z (n \text{ l\acute{o}p in}) = n\varepsilon_{inh-z} - \frac{(n-1)d}{h} \varepsilon_{inh-z} \end{cases} \quad (2.32)$$

2.4.2. Single-layer Printing Process

After depositing the first powder layer onto the build plate, the laser source begins heating according to a pre-set trajectory. The figure below illustrates the heat transfer zone during a single-track scanning process from left to right.

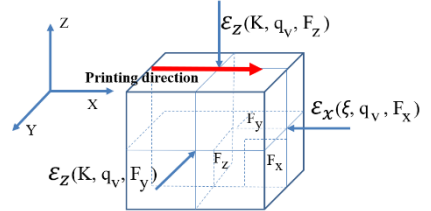


The temperature regions are color-coded from blue to dark red, representing the range from the initial temperature of the metal powder to its melting point. The dark red area in the figure indicates the current position of the laser beam spot. The yellow-orange-red zone is in the heating and melting phase. Here, the metal powder transitions from a solid to a liquid state, forming a "molten pool". The light blue to yellow zone is where the laser has already passed and is currently in the cooling and solidification phase. This rapid cooling process causes the material to transition from liquid back to solid at a lower temperature. This sudden thermal change subjects the printed part to compressive forces, leading to the formation of three-dimensional inherent strain (IS), defined as follows:

$$\varepsilon_x^* = \frac{W_x}{F_x}; \varepsilon_y^* = \frac{W_y}{F_y}; \varepsilon_z^* = \frac{W_z}{F_z} \quad (2.23)$$

Where: F_x , F_y , and F_z are the areas of the Heat Affected Zones (HAZ) where the quantities W_x , W_y , and W_z are distributed. The values of W_x , W_y , and W_z are calculated as follows:

$$W_x = \xi \cdot q_v; W_y = W_z = K \cdot q_v \quad (2.24)$$



In the above formula, q_v is the linear energy density (J/mm).

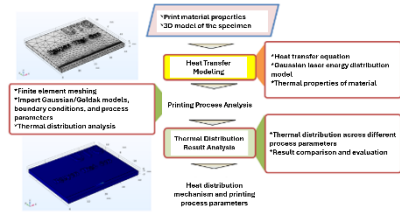
$$q_v = \frac{Q_{heat\ source}}{v} \quad (2.25)$$

The values ξ and K (mm/J) are the longitudinal and transverse inherent strain coefficients, respectively. The inherent strains in the x, y and z directions for the first layer are calculated as follows:

$$\varepsilon_{inh-x} = -\frac{\xi \cdot q_v}{F_x}; \varepsilon_{inh-y} = -\frac{K \cdot q_v}{F_y}; \varepsilon_{inh-z} = -\frac{K \cdot q_v}{F_z} \quad (2.26)$$

2.5. Printing process parameters affecting product quality

There are many factors affecting the quality of printed products, which can be categorized into four groups: material-related factors (e.g., particle size distribution, thermal properties); machine and printing method-related factors; printing condition-related factors (e.g., powder drying, substrate preheating, and post-processing methods); and printing process parameters. In this study, the process parameters include laser power U , layer thickness t , and scanning speed V . These are considered the primary parameters affecting dimensional accuracy, surface quality, and the microstructural characteristics of Ti6Al4V powder materials when using the SLM method.



2.6. Simulation methodology for investigating printing parameters

The simulation method allows for the identification of a suitable range of technological parameters to support experimental research. Via the simulation of the temperature field during printing, changes can be observed when the values of the technological parameters are altered.

The heat distribution mechanism and the set of printing parameters were determined using Comsol software, involving steps from setting up the heat transfer model and analyzing the printing process to analyzing the heat distribution results. During the heat transfer model setup phase, models such as the Gaussian model and the Goldak model—which represent the distributed laser energy—and material properties are input into the Comsol environment. To analyze the printing process, the Finite Element Method is applied; the printing model is meshed for analysis, and boundary conditions as well as technological parameters are established. The heat distribution results with different parameter sets, such as laser power, scanning speed, and layer thickness, are used to determine the appropriate set of technological parameters.

2.7. Experimental design methodology 2^k

2.7.1. Experimental design

The primary objective of selecting the experimental design (DOE) method is to answer the question: at which value levels and in which combinations do the factors in the experiment interact.

Experiments in which the number of levels for all factors is the same, and all combinations are used in the study, are called Full Factorial Design (FFD).

If the number of levels for each factor is 2, and the number of factors is k , the number of experiments to be performed is $N=2^k$. According to the results of a 2^k Full Factorial Design, a linear regression equation can be obtained:

$$y=b_0+b_1x_1+b_2x_2+\dots+b_kx_k \tag{2.33}$$

This equation can be supplemented with interaction terms between factors, denoted as $b_{ij}x_i x_j$

Fractional Factorial Design (FFD) allows for a reduction in the number of primary experiments compared to Full Factorial Design in cases where the number of terms in the regression equation is significantly smaller than the total number of primary experiments $N=2^k$.

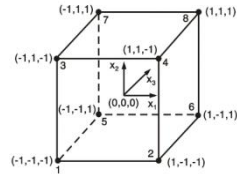
2.7.2. Full Factorial Design 2^k

For an FFD with 3 factors, denoted as 2^3 , the design matrix with the factors is presented in the following table:

N	Natural Factors			Coded Factors			Results
	X ₁	X ₂	X ₃	x ₁	x ₂	x ₃	
1	X _{1min}	X _{2min}	X _{3min}	-1	-1	-1	y ₁
2	X _{1max}	X _{2min}	X _{3min}	+1	-1	-1	y ₂
3	X _{1min}	X _{2max}	X _{3min}	-1	+1	-1	y ₃
4	X _{1max}	X _{2max}	X _{3min}	+1	+1	-1	y ₄
5	X _{1min}	X _{2min}	X _{3max}	-1	-1	+1	y ₅
6	X _{1max}	X _{2min}	X _{3max}	+1	-1	+1	y ₆
7	X _{1min}	X _{2max}	X _{3max}	-1	+1	+1	y ₇
8	X _{1max}	X _{2max}	X _{3max}	+1	+1	+1	y ₈

This table indicates the conditions for conducting the experiments. The sequence of experiments does not necessarily follow the order in the table but rather is chosen for convenience in setting factor values.

The vertices of the rectangular prism in Figure 2.22 represent the experimental levels. In coded form, these vertices correspond to the vertices of a unit cube. When the number of factors $k > 3$, geometric representation becomes very useful for visualization but difficult to present on paper.



General forms of the Regression Equations:

- Without interaction:

$$y=b_0+b_1x_1+b_2x_2+\dots+b_kx_k \tag{2.33}$$

- With interaction terms:

$$y=b_0+b_1x_1+b_2x_2+\dots+b_kx_k+b_{12}x_1x_2+b_{13}x_1x_3+\dots+b_{(k-1)k}x_{(k-1)}x_k \tag{2.37}$$

In this study, a 2^3 Full Factorial Design is used, in addition to the three dual interaction coefficients x_1x_2 , x_1x_3 , x_2x_3 there is also a triple interaction $x_1x_2x_3$, which is referred to as a second-order interaction. The model then takes the form:

$$y=b_0+b_1x_1+b_2x_2+b_3x_3+b_{12}x_1x_2+b_{13}x_1x_3+b_{23}x_2x_3+b_{123}x_1x_2x_3 \tag{2.38}$$

To determine the coefficients in the Regression Equation of an FFD, the Least Squares Method is used. Applying this method requires solving a system of equations with p unknowns (p là hệ số PTHQ).

The regression model can also be expressed in power-law form as follows:

$$D = aU^bV^c t^d \tag{2.42}$$

Where a , b , c , d are the model parameters from the experiment.

Taking the logarithm of both sides of equation 4.3, we have:

$$\ln(D) = \ln(a) + b \ln(U) + c \ln(V) + d \ln(t) \tag{2.43}$$

Setting $y = \ln(D)$; $x_1 = \ln(U)$; $x_2 = \ln(V)$; $x_3 = \ln(t)$ can obtain:

$$y = \beta_0 + \beta_1 x_1 + \beta_2 x_2 + \beta_3 x_3 \quad (2.44)$$

With $\beta_0 = \ln(a)$; $\beta_1 = b$; $\beta_2 = c$; $\beta_3 = d$

The design matrix X, is defined as follows:

$$X = \begin{bmatrix} \mathbf{1} & x_{11} & x_{12} & x_{13} \\ \mathbf{1} & x_{21} & x_{22} & x_{23} \\ \mathbf{1} & x_{31} & x_{32} & x_{33} \\ \vdots & \vdots & \vdots & \vdots \end{bmatrix} \quad (2.45)$$

Output vector y:

$$y = \begin{bmatrix} y_1 \\ y_2 \\ y_3 \\ \vdots \end{bmatrix} \quad (2.46)$$

Values of the parameters:

$$\text{With } \beta = [\beta_0, \beta_1, \beta_2, \beta_3]$$

The β values are determined as follows (OLS formula): Ordinary

Least Squares method [72].

$$\beta = (X^T X)^{-1} X^T y \quad (2.47)$$

Then, the values of a, b, c, d are determined as follows:

$$a = e^{\beta_0}; b = \beta_1; c = \beta_2; d = \beta_3 \quad (2.48)$$

2.7.3. Centerpoint in 2^k experimental design

In a 2^k experimental design, the centerpoint is the experimental point where all factors are set at the average level of the selected experimental range. The low and high (coded) values of each variable are ± 1 ; respectively; the center points are m measurements performed when all variables are equal to 0 This design consists of $2^k + m$ points with $m > 0$ [67].

Conclusion of chapter 2

Based on the content presented in Chapter 2, the following conclusions can be drawn:

1- The analysis of the SLM printing mechanism and the material phase transformations according to the temperature field serves as the basis for identifying the formation mechanism of thermal residual stress. This stress is the primary cause of part deformation when removed from the base plate. The analysis also establishes methods for determining residual stress values during single-layer and multi-layer printing.

2- A heat transfer model for the printing process was developed, incorporating coefficients representing temperature-dependent material thermal properties. Additionally, the heat source dissipation and the heat transfer efficiency from the laser source to the material melt pool were determined.

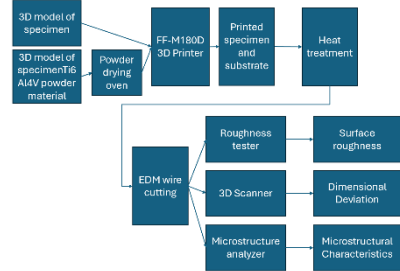
3- Analysis of laser heat source models, such as Gaussian and Goldak, provided the foundation for solving the heat transfer equations to determine temperature values during 3D printing.

4- Identified the printing process parameters that affect the laser volumetric energy density, influencing the printing process and subsequently impacting the final print quality.

CHAPTER 3. EXPERIMENT SYSTEM AND RESEARCH METHODOLOGY

3.1. Equipment system used in the research

To evaluate the geometric accuracy, surface roughness, and microstructural characteristics of the printed samples, the experiment steps and the necessary equipment system are illustrated in Figure 3.1. Ti6Al4V powder material is dried at a temperature of 200 °C. The 3D model of the printed sample is layer sectioned on computer and a G-code file is generated to be transferred to the printer. An FF-M180D 3D printer is used to print the samples. After printing, the sample and the base plate are annealed to relieve thermal residual stresses generated during the printing process. To separate the printed sample from the base plate, a Wire EDM (Electrical Discharge Machining) machine is used. To obtain the output parameters for geometric accuracy, surface roughness, and microstructural characteristics, a 3D scanner, surface profilometer, and microstructural analysis equipment are utilized, respectively.



3.1.1. SLM 3D Printer

Based on the simulation results from ComsolTM software, the experimental samples were produced on the FF-M180D SLM metal 3D printer.



Figure 3.2. FF-M180D metal SLM 3D printer manufactured by 3D HONY

Specification	Value
Build area	Diameter 180 mm, height 100 mm
Base plate setup	Magnetic fixation
Accuracy	±0.05mm
Layer thickness	0.02-0.06 mm
Powder spreading method	Bidirectional powder feeding and spreading
Spreading blade type	Rubber recaster
Maximum powder load	50kg
Printable materials	CoCr, TiAl, Ti
Number of lasers	Dual-laser system, supports single-laser operation
Laser power	1000W (two lasers 500W)
Cooling method	Water
Laser beam diameter	50-80µm
Protective gas	Ar/Nitrogen
Minimum oxygen level	0.01%
Energy consumption	3kW
Scanning speed	0-7m/s

Figure 3.2 shows the overall setup of the FF-M180D 3D printer using the SLM (Selective Laser Melting) method. The main technical specifications of the machine are presented in Table 3.1, featuring a maximum cylindrical print size of D 180mm, H 100mm; a laser source power of 1000W; and a layer thickness of 0.02-0.06 mm.

3.1.2.-3.1.4. Experiment equipment



Figure 3.5. Wire EDM machine and schematic diagram of the cutting principle

Figure 3.4. FF-M180D metal SLM 3D printer

Figure 3.5. Thermoelectric furnace

3.1.5. Ti6Al4V Powder

Ti6Al4V titanium alloy powder, with a particle size distribution largely ranging from 25 μm to 63 μm was used to print the samples. The percentage distribution of particle diameters (d') is as follows: $d' \leq 25$ accounts for 0.8%; d' in the range of 25 μm to 63 μm accounts for 83.4%; and $d' > 63$ μm accounts for 15.8%. The material used in the experiment was obtained directly from 3D HONY Company.

3.1.6. Experimental Samples

The shape and dimensions of the samples are shown in Figure 3.8. The sample dimensions (length x width x height) are 40x32x3 (mm), respectively.

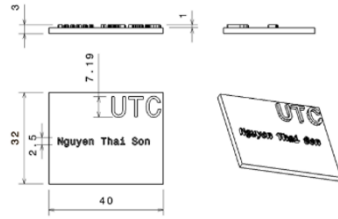
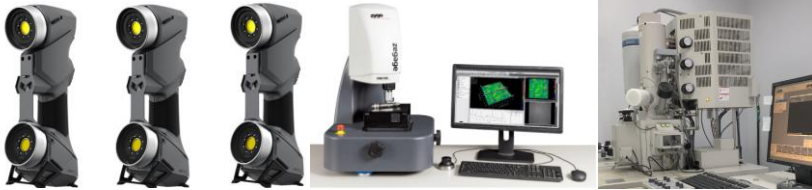


Figure 3.8. Dimensions and geometry of the experimental specimen

3.2. Equipment for Product Quality Assessment

This includes equipment and software used to evaluate geometric accuracy, equipment to assess the mechanical properties of the printed samples, and measurement devices (Handy Scan 3D Silver by Creaform, Zygo Zegage Pro HR surface profilometer, and HITACHI FESEM S4800).



3.3. Research Methodology

3.3.1. Simulation Methodology

In this study, the established thermal model accounts for material properties and printing process parameters including laser power, scanning speed, layer thickness, and printing environment conditions. The numerical simulation result is the temperature field during printing (as shown in Figure 3.15). The set of printing process parameters is considered suitable for the printing process when it creates a temperature field within a range higher than the material's melting point and lower than the material's evaporation temperature.

3.3.2. Experimental Methodology

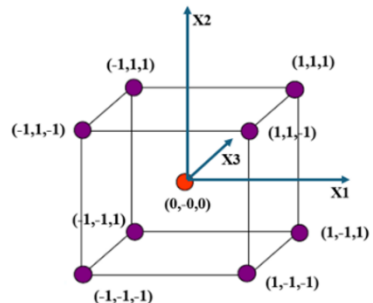


Figure 3.16. Three-factor two-level full factorial design [105, 106]

The most widely used Design of Experiments (DOE) method is the Full Factorial Design. An experiment in which all factors are varied across the same number of levels, and all possible combinations are studied, is called a full factorial experiment. In experimental design theory, full factorial designs offer several advantages over other planning methods, such as: independent estimation of regression coefficients; minimized variance; and simplified experimental data processing. With k factors, each having

2 levels (the minimum and maximum values of the factor) the required number of main experiments is $N = 2^k$ [66]. Furthermore, to evaluate the non-linearity of the response function y , one center point experiment is added [67]. Figure 3.16 illustrates the design space for a 3-factor experiment with two full levels, totaling 9 experimental runs. Based on the results of the 2^k full factorial experiment, a first-order regression equation can be obtained as follows:

$$y = b_0 + b_1x_1 + b_2x_2 + \dots + b_kx_k + \sum b_{ij}x_i x_j \quad (3.1)$$

The above equation accounts for both the main effects of individual factors and the interaction effects between factors on the output response y .

In this context, for the centerpoint experiment (Run 9), the factor values are the arithmetic mean of the two levels for each factor..

In this study, with 3 input parameters—laser power, scanning speed, and layer thickness—9 experiments were conducted. The experimental output data includes surface roughness, geometrical deviation, and microstructural characteristics.

Conclusion of Chapter 3

From the contents of Chapter 3, the following conclusions are drawn:

1-The 3-factor experimental design process with the following input parameter boundary values:

$$150 \leq \text{laser power} \leq 350 \text{ (W)}$$

$$400 \leq \text{scanning speed} \leq 1500 \text{ (mm/s)}$$

$$\text{Layer thickness} \leq 0.06 \text{ (mm)}$$

2- Through numerical simulation, the aforementioned set of process parameters is found to be appropriate as the thermal field values during printing show that the maximum generated heat exceeds the melting temperature but remains below the boiling point of the Ti6Al4V material

3- The equipment system, comprising the additive manufacturing (3D printing) system and post-processing data analysis equipment, has been identified and verified to ensure the successful execution of experimental plans and data processing. This serves as the foundation for achieving the objective of determining the relationship between technological parameters and product quality indicators, as presented in Chapter 4.

Table 3.7. Full factorial design with three coded factors

N	Natural Factors			Coded Factors			Results
1	X _{1min}	X _{2min}	X _{3min}	-1	-1	-1	y ₁
2	X _{1max}	X _{2min}	X _{3min}	+1	-1	-1	y ₂
3	X _{1min}	X _{2max}	X _{3min}	-1	+1	-1	y ₃
4	X _{1max}	X _{2max}	X _{3min}	+1	+1	-1	y ₄
5	X _{1min}	X _{2min}	X _{3max}	-1	-1	+1	y ₅
6	X _{1max}	X _{2min}	X _{3max}	+1	-1	+1	y ₆
7	X _{1min}	X _{2max}	X _{3max}	-1	+1	+1	y ₇
8	X _{1max}	X _{2max}	X _{3max}	+1	+1	+1	y ₈
9	X ₁₀	X ₂₀	X ₃₀	0	0	0	y ₉

CHAPTER 4: RESEARCH ON THE EFFECTS OF SLM PROCESS PARAMETERS ON OUTPUT INDICATORS

4.1. Introduction

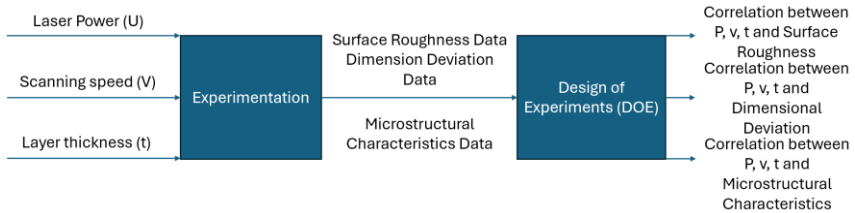
Based on the analysis of how process parameters—including laser power, scanning speed, and layer thickness—affect the temperature field distribution during printing through numerical methods and Finite Element Analysis (FEA) as mentioned in Chapters 2 and 3. When these technological parameters are varied, the temperature field values change accordingly.

From the simulation analysis results, to ensure that the printing temperature remains within the range of being higher than the material's melting point and lower than its boiling point, the determined set of process parameters includes:

$$150 \leq \text{laser power} \leq 350 \text{ (W)}$$

$$400 \leq \text{Scanning speed} \leq 1500 \text{ (mm/s)}$$

$$0.03 \leq \text{layer thickness} \leq 0.06 \text{ (mm)}$$



4.2. Experimentation

4.2.1. Purpose of the experiment

The experimental study was conducted to determine the influence of technological parameters, including laser power, printing speed, and layer thickness, on the output quality indicators, namely shape deviation, surface roughness, and microstructural characteristics of parts fabricated on an SLM 3D printer using Ti6Al4V powder material.

4.2.2. Experimental design

In this study, 3 technological parameters were selected for investigation, including laser power (W), scanning speed (mm/s), and layer thickness (mm). In order to evaluate the influence of process parameters on printing quality, a full two-level factorial experiment with 03 factors was used to design the experiments. 8 experimental samples and 01 center-point experiment were carried out with different values of the 3 parameters mentioned above. The experimental design is presented in Table 4.1.

Bảng 4.1. Bộ thông số công nghệ in SLM

STT	Công suất nguồn laser (W)	Vận tốc in (mm/s)	Chiều dày lớp in (μm)
1	150	400	30
2	350	400	30
3	150	1500	30
4	350	1500	30
5	150	400	60
6	350	400	60
7	150	1500	60
8	350	1500	60
9	250	950	45

4.2.3. Experimental procedure

4.2.3.1. Printing of samples

Based on the data from the experimental design, the printed samples were fabricated on the SLM metal 3D printer FF-M180D.



The Ti6Al4V alloy powder was preheated to 200 °C before printing.

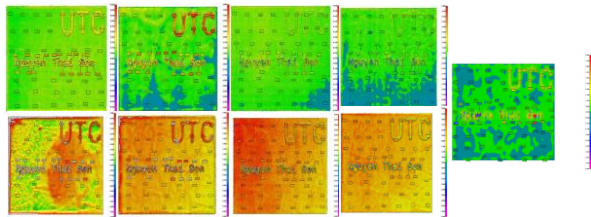
After the printing process was completed, the printed samples were separated from the substrate using a wire electrical discharge machining (EDM) machine.

4.2.3.2. Measurement of shape deviation

To determine the shape deviation of the printed samples, the samples were scanned in 3D. The 3D scan data of each sample were compared with the original CAD 3D model.

The steps for determining the shape deviation of the printed samples are shown in Figure 4.2.

To generate 3D models of the printed samples, a HandySCAN



3D scanner using non-contact 3D scanning technology was used.

The printed samples were scanned, and the scan data were obtained in the form of point clouds. Geomagic software was used to process the point cloud data into surface models. These surface models were then converted into solid models to be compared with the original CAD model in order to determine the shape deviation.

The results of shape deviation measurements for the samples are shown in the figure, in which red corresponds to positive deviation (sample dimensions larger than the required dimensions), blue corresponds to negative deviation (sample dimensions smaller than the required dimensions), and green corresponds to zero deviation (sample dimensions equal to the required dimensions).

4.2.3.3. Measurement of surface roughness

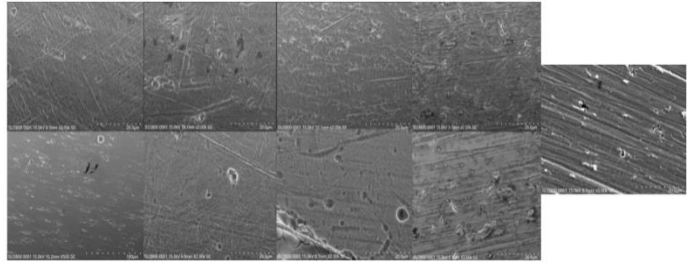
To determine the surface roughness of the printed samples, the Zygo Zgage Pro HR measurement system at the Military Technical Academy was used. The steps for determining surface roughness are shown in Figure 4.5. To improve measurement accuracy, each printed sample was measured at 3 measurement regions, and the surface roughness value was calculated as the average value of these 3 measurement regions.

For the 9 printed samples, each sample was measured at 3 different regions with surface roughness parameters including Ra, Sa, and Sz, as shown in Table 4.5. In this study, the Ra parameter was used to evaluate the surface roughness of the printed samples.

4.2.3.4. Microstructural characteristics

Microstructural characteristics play a decisive role in the mechanical, chemical, and thermal properties of materials. In this study, via microstructural examination using the FESEM S4800 HITACHI system at Hanoi University of Industry, defects and pores in the printed samples at the micrometer scale were evaluated.

ImageJ software was used to process the images, thereby allowing the porosity and density of the printed samples to be evaluated.



The

microstructural examination results for the samples are shown in the corresponding figures.

4.3. Results and discussion

4.3.1. Effect of printing process parameters on shape deviation

With the objective of establishing a regression model representing the relationship between the printing process parameters and the output parameter, namely the shape deviation of the printed samples, the 3D scanning data of the printed samples were processed and analyzed. The maximum shape deviation value (D) of each printed sample is presented in Table 4.7.

Table 4.7. Maximum dimensional deviation results of printed specimens

Specimen	Laser Power U (W)	Scanning Speed (mm/s)	Layer thickness t (mm)	Max Dimensional Deviation D (mm)
1	150	400	0.030	0.319
2	350	400	0.030	0.611
3	150	1500	0.030	0.142
4	350	1500	0.030	0.121
5	150	400	0.060	0.682
6	350	400	0.060	0.664
7	150	1500	0.060	0.447
8	350	1500	0.060	0.370
9	250	950	0.045	0.417

The regression equation for shape deviation is expressed as follows:

$$D = 376.908 U^{0.162} V^{-0.595} t^{1.217}$$

4.3.2. Effect of printing process parameters on surface roughness

Based on the experimental results, the measured surface roughness values Ra (1D) and Sa (2D) are presented in Table 4.11.

The regression equations for surface roughness are given as follows:

Table 4.11. Measured roughness value Ra, Sa results of printed specimens

Specimen	Laser Power U (W)	Scanning Speed (mm/s)	Layer thickness t (mm)	Roughness value Ra (μm)	Roughness value Sa (μm)
1	150	400	0.03	5.088	4.840
2	350	400	0.03	3.319	4.717
3	150	1500	0.03	13.902	12.886
4	350	1500	0.03	15.751	15.588
5	150	400	0.06	6.553	9.071
6	350	400	0.06	7.198	7.558
7	150	1500	0.06	24.025	20.610
8	350	1500	0.06	10.362	11.924
9	250	950	0.045	7.407	6.745

$$R_a = 1.0005 U^{-0.329} V^{0.781} t^{0.397}$$

$$S_a = 1.6372 U^{-0.194} V^{0.627} t^{0.442}$$

4.3.3. Effect of printing process parameters on porosity

From the microstructural examination results of the printed samples, defects such as pores caused by incomplete melting of powder material and unmelted particles were observed in some samples. The detailed results are presented in Table 4.16.

The regression equation for porosity is expressed as follows:

$$P = 49.853 U^{-0.284} V^{0.181} t^{0.548}$$

4.4. Optimal printing process parameters

4.4.1. Optimal printing process parameters for single-objective quality optimization

The minimum shape deviation was obtained at $U = 150$ W; $V = 1500$ mm/s, and $t = 0.03$ mm.

The minimum surface roughness and minimum porosity were obtained at $U = 350$ W; $V = 400$ mm/s, and $t = 0.03$ mm.

4.4.2. Optimal printing process parameters for multi-objective quality optimization

In the consideration of printing process parameters to achieve multiple quality objectives, including minimum shape deviation, minimum surface roughness, and minimum porosity.

$$\begin{cases} D = 376.908 U^{0.162} V^{-0.595} t^{1.217} \rightarrow \min \\ R_a = 1.0005 U^{-0.329} V^{0.781} t^{0.397} \rightarrow \min \\ P = 49.853 U^{-0.284} V^{0.181} t^{0.548} \rightarrow \min \end{cases}$$

The printing process parameters for achieving the multi-objective optimization problem are $U = 341.919$ W; $V = 400$ mm/s, and $t = 0.03$ mm.

Conclusions of Chapter 4

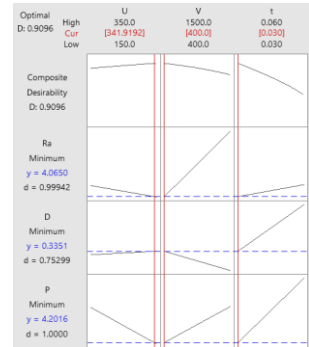
From the content and results of Chapter 4, the following conclusions can be drawn:

1-From the experimental design, the relationships between the output quality indicators and the input process parameters were established. The shape deviation decreased with increasing scanning speed; when the layer thickness is small, shape deviation decreases with increasing printing speed, and the average laser power within the investigated range is from 150 W to 350 W.

2- With a layer thickness of $t = 0.03$ mm, the printed parts exhibited shape deviation values smaller than 0.2 mm when the printing speed was in the range

Table 4.16. Measured porosity results of printed specimens

Specimen	Laser Power U (W)	Scanning Speed (mm/s)	Layer thickness t (mm)	Relative Density (%)	Porosity (%)
1	150	400	0.03	92.190	7.810
2	350	400	0.03	96.220	3.780
3	150	1500	0.03	95.419	4.581
4	350	1500	0.03	92.978	7.022
5	150	400	0.06	92.655	7.345
6	350	400	0.06	94.435	5.565
7	150	1500	0.06	87.625	12.375
8	350	1500	0.06	90.452	9.548
9	250	950	0.045	96.437	3.563



of $V = 1250$ mm/s to 1500 mm/s and the laser power was in the range of $U = 150$ W to 350 W.

3- For layer thicknesses of $t = 0.05$ mm and $t = 0.06$ mm, achieving shape deviation values smaller than $D = 0.3$ mm required higher values of both laser power and printing speed. In this study, the maximum shape deviation of 0.682 mm occurred at the printing parameters $U = 150$ W, $V = 400$ mm/s, and $t = 0.06$ mm.

4- The optimal printing process parameters for minimizing shape deviation were identified as $t = 0.03$ mm, $U = 350$ W, and $V = 1500$ mm/s, corresponding to a minimum shape deviation of $D = 0.1207$ mm.

5- An increase in scanning speed V and layer thickness t resulted in higher surface roughness R_a values, whereas increasing the laser power U led to a reduction in surface roughness. Higher laser power enhanced the melting of metal powder, thereby improving the surface quality of the printed parts.

6- Among the printed samples, the lowest surface roughness value of $R_a = 3.319$ μm was obtained at the printing parameters $U = 350$ W, $V = 400$ mm/s, and $t = 0.03$ mm. This sample exhibited the most uniform microstructure with only a small number of fine pores. In contrast, the highest surface roughness value of $R_a = 24.025$ μm was observed at $U = 150$ W, $V = 1500$ mm/s, and $t = 0.06$ mm, corresponding to a microstructure containing numerous defects such as large pores and coarse unmelted particles.

7- When considering multiple quality objectives simultaneously, including minimum shape deviation, minimum surface roughness, and minimum porosity, the optimal set of printing process parameters was determined to be $U = 350$ W, $V = 500$ mm/s, and $t = 0.03$ mm.

GENERAL CONCLUSIONS AND FUTURE RESEARCH DIRECTIONS

a) General conclusions

Based on the content and results obtained in this dissertation, the following general conclusions can be drawn:

1- Considering the material characteristics, the phase transformation of the material under the thermal field was analyzed as a basis for determining appropriate printing process parameters to achieve a melting temperature of Ti6Al4V higher than 1877 K and lower than the evaporation temperature of 3533 K. In addition, the temperature-dependent thermal properties of the material, such as specific heat capacity and thermal conductivity, as well as their variations during phase transformation, were identified.

2- For the SLM printing process, the printing mechanism was analyzed to determine the thermo-mechanical-chemical behavior of the material during printing. A heat transfer model was developed with key parameters including material properties (specific heat capacity and thermal conductivity) and

printing parameters (scanning speed and laser power). Furthermore, the thermal source model and thermal energy losses were identified.

3- Regarding printing conditions, pre-printing treatments (preheating the powder to 200 °C) and post-printing treatments (heat treatment of both the printed samples and the substrate) were applied in order to reduce residual thermal stresses generated during the printing process.

4- With respect to printing process parameters, the effects of laser power, layer thickness, and scanning speed on surface roughness, shape accuracy, and microstructural characteristics were investigated. Based on the relationship between printing parameters and quality indicators, the following results were obtained:

- A heat transfer equation for the SLM printing process was established, in which the dissipated energy components were identified. The heat transfer equation using a Gaussian-distributed laser heat source model was applied to generate the temperature field during printing. The temperature field is a critical basis for determining the required laser energy and appropriate printing process parameters.

Mathematical models describing the relationships between shape deviation (D), surface roughness (R_a), and porosity with the printing process parameters, including laser power U , printing speed V , and layer thickness t , were established.

- Optimal printing process parameters satisfying both single-objective and multi-objective optimization problems were determined, achieving minimum shape deviation, minimum surface roughness, and maximum density simultaneously.

b) Future research directions

Based on the results obtained in this dissertation, future research directions include developing in-situ quality monitoring and control during the printing process through the application of artificial intelligence in order to reduce printing defects, as well as conducting further studies on 3D printing of parts with complex surface geometries.

LIST OF PUBLICATIONS RELATED TO THE THESIS

1. Tran Ngoc Hien, **Nguyen Thai Son**, Prediction of part distortion in metal. 3D printing. Tạp chí Cơ khí Việt Nam, số 6, năm 2021, trang 225-229
2. Ngoc-Hien Tran and **Thai-Son Nguyen**, “Calculating the Inherent Strain in 3D Printed Part Based on the Heat Affected Zone”, In: Long, B.T., et al. Proceedings of the 3rd Annual International Conference on Material, Machines and Methods for Sustainable Development (MMMS 2022). Lecture Notes in Mechanical Engineering. Springer, Cham. https://doi.org/10.1007/978-3-031-31824-5_12, Scopus.
3. **Nguyễn Thái Sơn**, Trần Ngọc Hiền, “Nghiên cứu thực nghiệm về ảnh hưởng các thông số công nghệ in 3D kim loại đến chất lượng sản phẩm in”, Tạp chí Cơ khí số 309, tháng 11, 2023.
4. **Thai-Son Nguyen** and Ngoc-Hien Tran, “Study on optimization of 3D printing parameters for part quality”, Proceedings of the 4th Annual International Conference on Material, Machines, and Methods for Sustainable Development (MMMS2024), <https://doi.org/10.1007/978-031-93816-0-8>, Scopus.
5. Ngoc-Hien Tran, **Thai-Son Nguyen**, Chapter 6: Additive Manufacturing and 3D Printing Revolution in Industry 5.0. In Book: Digital Manufacturing in Industry 5.0; Publisher: Springer Nature; Editor: Dr. Yogesh Kumar Singla, Dr. Ashwani Kumar, Dr. Michael R. Maughan; ISBN-13.978-3031914997; Publication date: 23 Jan. 2026.
6. **Nguyễn Thái Sơn**, Nguyễn Chí Sáng, Trần Ngọc Hiền, Nghiên cứu mô phỏng phân bố nhiệt trong công nghệ sản xuất bồi đắp. Tạp chí Cơ khí Việt Nam; số 331, 2025.
7. **T. S. Nguyen** and N. H. Tran, “An Experimental Investigation of the Shape Deviation of SLM Printed Parts”, Eng. Technol. Appl. Sci. Res., vol. 15, no. 5, pp. 26757–26764, Oct. 2025. <https://doi.org/10.48084/etasr.12777>
Thai-Son Nguyen, Ngoc-Hien Tran, Surface Roughness and Microstructure Characterization of the SLM printed Parts. EUREKA: Physics and Engineering, Scopus, 5(60), 117-131. <https://doi.org/10.21303/2461-4262.2025.0039>